

Freezing Suppression in Confined Water

TÁSSYLLA O. FONSECA

PATRICIA TERNES

Instituto de Física, Universidade Federal do Rio Grande do Sul,
CEP 91501-970 Porto Alegre, RS, Brazil.

ALAN B. DE OLIVEIRA

Departamento de Física, Universidade Federal de Ouro Preto,
CEP 35400-000 Ouro Preto, MG, Brazil.

MARCIA C. BARBOSA

Instituto de Física, Universidade Federal do Rio Grande do Sul,
CEP 91501-970 Porto Alegre, RS, Brazil.

Abstract

We study confined water in cellulose matrix through Monte Carlo simulations. To determine the crystal-fluid transition temperature behavior for confined water, we vary the diameter and length of channel, and the nature of wall-water interaction. Our model presents a transition temperature dependent with the channel diameter and independent of channel length. The transition temperature is larger for hydrophobic walls than hydrophilic walls. In the hydrophilic case one fluid layer in wall-water interface is observed. The transition temperature also depends of water latent heat value. In hydrophobic systems the transition temperatures reaching the bulk water transition temperature, for higher latent heat used. In all situations analyzed the confined water transition temperature is lower than the bulk water transition value.

1 Introduction

Water has very peculiar behaviors not observed in other liquids. For instance, the density at room pressure has a maximum at 4° C [1, 2, 3] while in most materials the density increases monotonically with the decrease of the temperature. In addition, between 0.1 MPa and 190 MPa water also exhibits an increase of compressibility [4, 5] and, at atmospheric pressure, an increase of isobaric heat capacity upon cooling. [6, 7] In addition to these thermodynamic anomalies water also presents an unusual behavior in its mobility. The diffusion coefficient that for normal liquids increases with the decrease of pressure, for water it has a maximum at 4° C for 1.5 atm. [3, 8]

The presence of the large increase in the response function led to the hypothesis of the existence of two liquid phases and a critical point. [9] Unfortunately this liquid-liquid coexistence is located at

the supercooled region beyond the line of homogeneous nucleation what makes the its experimental observation a challenge. In order to circumvent this inconvenience, experiments in confined water were performed. [10, 11] They showed that the large increase of the specific heat it is actually a peak that can be associated with the Widom line. This line is found [11] as the continuation of the liquid-liquid coexistence line beyond the critical point at the one phase region. [10, 11]

The drawback of experiments in nanoscale confinement is that the results obtained do not necessarily lead to conclusions at the bulk level. In fact new physical observations arise when studying confined systems. These new results are important for understanding a number of confined systems. One particular example is water confined in the cellulose matrix. There is a scientific and technological race for the commercial scale production of second generation ethanol. Second generation ethanol is produced from lignocellulosic biomass. Lignocellulosic biomass is the most abundant renewable biological resource on earth. [12, 13] This refers to components such as: sugarcane straw, sugarcane bagasse, wood, components of corn, cotton, among others. [14, 15] The production of ethanol from cellulose can be done using “wastes” that are discarded by industry. So, it is possible increases ethanol production without increasing the extent of cultivated land. [16]

The conversion of biomass to ethanol has been considered a promising alternative to meet global demand for fuels. [12] There are technologies available for pulp processing, but most of them face technical or economic difficulties. [12, 14, 17, 18] Starting from the lignocellulosic biomass, there will be three processes until the ethanol is obtained. The first process is the pre-treatment where there extraction of cellulose from the basic components that make up the biomass, cellulose, lignin and hemicellulose. After the initial separation, the pulp undergoes a hydrolysis step, which leads to their “breaking” into glucose molecules. Finally, through fermentation and distillation, the cellulosic ethanol is obtained. [19]

In biofuel production, one important step is the cellulose washing. In addition to being used to remove sugars, water is also an instrument to evaluate the structure of the cellulose matrix through a process of thermoporometry. [20, 21] This experimental method consists of immersing the cellulose in water at room temperature and freezing it. After removal of the bath, the water is heated slowly. It is noted in this process that the fusion occurs at a different temperatures than the bulk temperature. Then the question arises of how the change in the freezing of confined water depends in the confining geometry and particularly on the confining diameter. If this relation could be found a method for finding the distribution of sizes inside the celulose matrix could be established.

Experimental and computational studies of freezing in nanochannels suggest that the crystal-fluid transition temperature of confined water is related to the nature of confinement (hydrophobic or hydrophilic walls) and the degree of confinement (confining channel size) [22, 23, 24, 25, 26, 27] and that not all water present in the channel can be crystallized. In some confining geometries pre-melted water has been observed in nanochannels experiments such as calorimetry, nuclear magnetic resonance, neutron diffraction, X-ray and Raman. [22, 23, 28, 29] However, the clear relation between the presence of a pre-melted layer and a shift in the melting temperature of the confined water is still not established.

In order to understand how the transition temperature of the confined water depends on the nature of the confining wall and the confinement size, we propose a model of cellulose nanochannels for confinement. This lattice model incorporates the fusion/solidification process in an approximate way. We also verify the relation between water structure in contact with wall and the confinement.

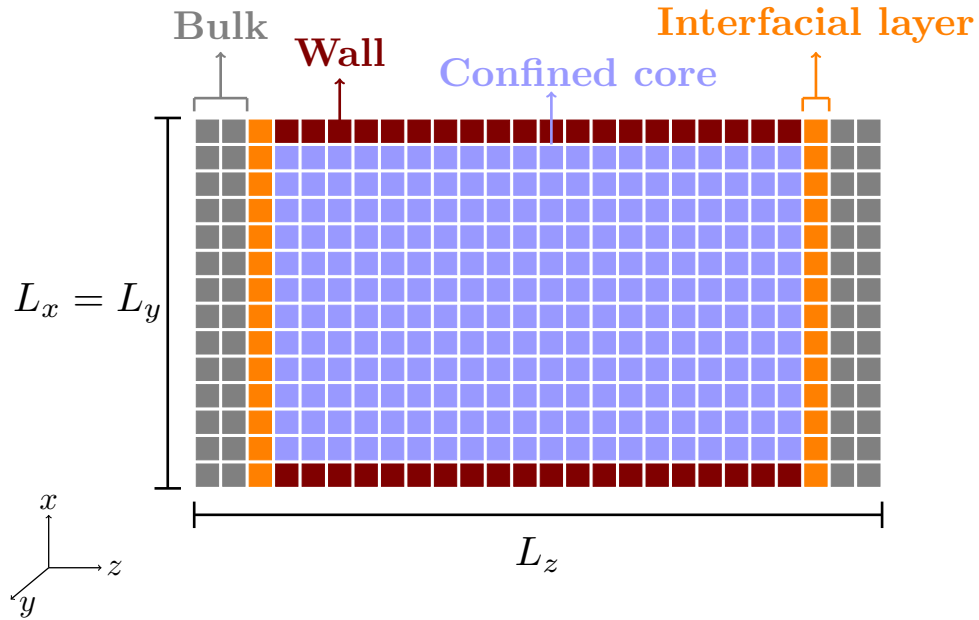


Figure 1: Schematic representation of the xy plane cross-section of the system structure. Dark red sites represents the nanopore wall (solid), gray sites represents bulk water (fluid or crystal), blue sites represents the confined water (fluid or crystal) and orange sites represents the water in the interfacial layer (fluid or crystal) between the bulk and the confined water.

The remaining of this paper goes as follows. In the section II the model and the simulation details are presented, results are analyzed in the section III and section IV shows the conclusions.

2 Lattice model

The system is defined on a parallelepipedic lattice, with volume $L_x^2 L_z$ which represents the confining geometry in contact with the bulk as illustrated in the Figure 1. In the channel two types of particles are present: the particles that make up the channel walls and the particles that represent the water. The channel ends in the z direction in one layer of interfacial water and two layers of water particles that represent the bulk water. All the sites inside the channel are either in the fluid or in the crystal state.

The state of the bulk water is fixed by the transition temperature, T_0 . For $T > T_0$ the bulk is in fluid state while for $T < T_0$ the bulk is in crystal state. The bulk acts as a local field in the interfacial layer, influencing its state. The state of the interfacial layer and the water within the confined core are defined according to a Monte Carlo statistic. The energy difference if a selected site is changed from the fluid to the crystal phase is given by the following Monte Carlo energy gap [30]

$$\Delta E = L \left\{ \frac{T}{T_0} - 1 + \frac{1}{6} \Delta N_{cf} + W_c \Delta N \right\}, \quad (1)$$

where L is the bulk latent heat which in addition to taking into account the degrees of freedom of hydrogen bonds (internal targeting of molecules), also includes van der Waals intermolecular interactions. L is

the heat required in the bulk at $T = T_0$ for the transition from the fluid to the crystal phase to occur. $\Delta N_{cf} = N_{cf}^c - N_{cf}^f$ is the difference between the numbers of first neighbors in the fluid phase when the selected site is in the crystal phase, N_{cf}^c , and the number of first neighbors in the crystal phase when the selected site is in the fluid phase, N_{cf}^f . $\Delta N_{cs} = N_{cs}^c - N_{cs}^f$ is the difference between the numbers of first neighbors which belong to the wall if the the selected site is in the crystal phase, N_{cs}^c , and the number of first neighbors in the wall when the selected site is in the fluid phase, N_{cs}^f . W_c is the water-wall interaction in units of latent heat. $W_c \leq 0$ represents a hydrophobic wall and $W_c > 0$ represents a hydrophilic wall.

In a typical bulk system, the crystal-fluid phase transition occurs when a crystal fragment of a certain critical size is formed and the volumetric energy of the crystal-crystal interactions of this fragment is less than the crystal-fluid interface. In a confined system, the interaction with the wall unbalances this competition between volume and surface, and the transition temperature changes. In the specific case of water, confinement has an additional effect. The hydrogen bonds are directional and the wall makes the formation of water-water bonds impossible. In some cases, the wall forms bonds with the water, thereby eliminating further formation of these bonds. The model used in this work is capable to describe the breakdown of water-water hydrogen bonds due the confinement and the formation of water-wall hydrogen bonds if the channel was hydrophilic.

Two different definitions of the density of the confined fluid water are employed. The total fluid density, ρ_{total} , includes all the water molecules in the fluid state divided by the total number of available sites. The central fluid density, $\rho_{central}$ includes only the central water molecules in the fluid state divided by the total number of available sites. This density excludes the water molecules at the contact layer and the interfacial water. If all the sites are in the fluid state $\rho_{total} = 1$ while if all the central sites are in the fluid state $\rho_{central} = 1$. Due to site conservation the densities of water in the crystal phase are $1 - \rho_{total}$ and $1 - \rho_{central}$. In resume, the fluid densities are given by

$$\rho_{total} = \frac{N_f}{M} \quad \text{and} \quad \rho_{central} = \frac{N_f^c}{M^c}, \quad (2)$$

where N_f is the number of sites in the fluid state belonging to the confined core and M is the total number of confined core sites. N_f^c is the number of sites in the fluid state belonging to the confined core without the sites of contact layers, and M^c is the total number of confined core sites without contact layers.

The evolution of the system was studied through Monte Carlo dynamics. We simulate the particles of the system inside a parallelepiped box in contact with a thermal bath at the temperature of T_0 . The particles belonging to the bulk had their state varied in accordance with the temperature T in relation to T_0 , equilibrium transition temperature of the bulk. The sites were maintained in the crystal state, when $T < T_0$, or in the state of fluid when $T > T_0$. We initiate the simulations with the confined particles plus the interfacial layer particles, between confined and bulk, in the crystal state, where T has an initial value below T_0 , then the bulk also starts in the crystal state. We will vary the number of confined particles, from $L_x = L_y = 5$ nm to $L_x = L_y = 60$ nm, maintaining $L_z = 13$ nm, in the case of simulations in which we wanted to observe the effect of the variation of the diameter of the nanopore at the confined water transition temperature. Another case where the effect of channel length variation on the confined water transition temperature was the interest, we have fixed $L_x = L_y = 7$ nm and we vary L_z , from $L_z = 7$ nm to $L_z = 17$ nm. We use the latent heat of fusion, L , from 6,006 to 20 kJ/mol and degree of hydrophilicity, W_c ,

from 0 (hydrophobic) to 10. During our simulations, we varied the temperature from 10 K to 300 K in the heating route, and from 300 K to 10 K in the cooling route. The balancing counted for 10^4 steps from Monte Carlo. The number of uncorrelation steps between one measure and another was 10^3 . The number of measures taken was 10^2 .

3 Results

In order to understand the effects of the presence of the wall in the thermodynamic properties of the confined water, the fluid-crystal transition temperature is computed as follows. The bulk system is fixed at the crystal phase and the Monte Carlo simulations are performed at $T < T_0$. The temperature is then raised at small time steps. Then, simulations at high temperatures $T > T_0$ in which the bulk water is in the fluid phase. Then the temperature is decreased also at small time steps.

Several parameter sets were tested: channel diameter, L_x , from 5 to 60 nm; latent heat of fusion, L , from 6.006 to 20 kJ/mol; and degree of hydrophilicity, W_c , from 0 (hydrophobic) to 10. The bulk water crystal-fluid transition temperature and the channel length were fixed in $T_0 = 273.15$ K and $L_z = 13$ nm, respectively, in all simulations.

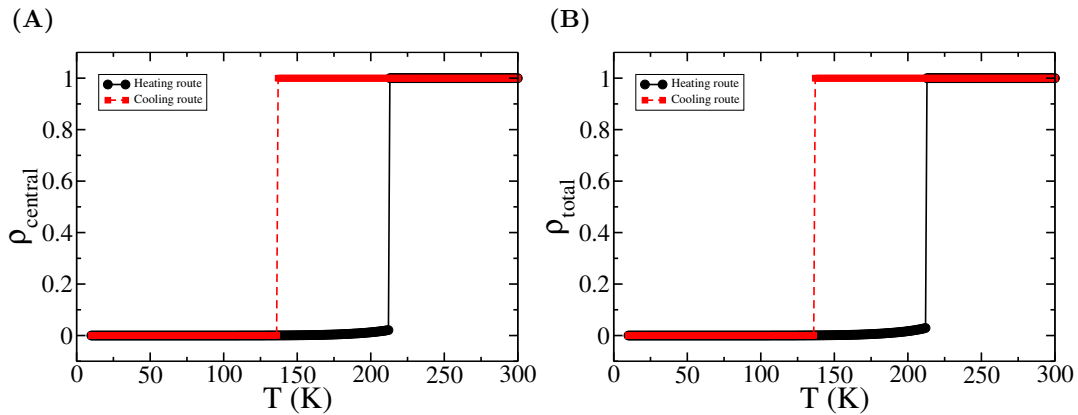


Figure 2: (A) Central ($\rho_{central}$) and (b) Total Fluid Density (ρ_{total}) versus temperature for $L_x = L_y = 7$ nm, $L_z = 13$ nm, $W_c = 0$, and $L = 6.006$ kJ/mol. The black solid curves are the heating routes and the red dashed curve are the cooling routes.

The Figure 2 shows the of fluid water density versus temperature for a confined system with channel diameter of $L_x = L_y = 7$ nm and channel length]of $L_z = 13$ nm, with water-wall interaction purely repulsive, that is, system hydrophobic $W_c = 0$, and latent heat of fusion, $L = 6.006$ kJ/mol (this is the latent heat of the crystal-fluid transition of bulk water). [31]

Comparing central and the total density of water molecules in the fluid phase it is possible to identify that there is no significant difference between ρ_{total} and $\rho_{central}$, which indicates that the wall is not wetted by the water, in other words the water-wall contact layer are not in fluid state when the confined system freezes.[32] This result implies that, for this model, hydrophobic walls ($W_c = 0$) do not suffer wettable.

The Figure 3 shows the water fluid density versus temperature for a confined system with dimensions of $L_x = L_y = 7$ nm and $L_z = 13$ nm, with hydrophilic wall, $W_c = 3$, and latent heat of fusion, $L = 6.006$ kJ/mol. Comparing the central and the total densities we can see a clear distinction between hysteresis curves for the two types of density. While in (A) the heating route starts with fluid water density equal to zero, in (B) the heating route starts with the fluid water density at a non-zero value: 0.3056. This is due to the fact that ρ_{total} associates the formation of a fluid water layer between the channel walls and the frozen core within the channel. We further analyze other values of W_c , 1.35, 2.10, 4.05, 5.25, 6.60, 8.10 and 9.75. For all these values of W_c , both fluid water densities, $\rho_{central}$ and ρ_{total} , behave similarly to $W_c = 3$.

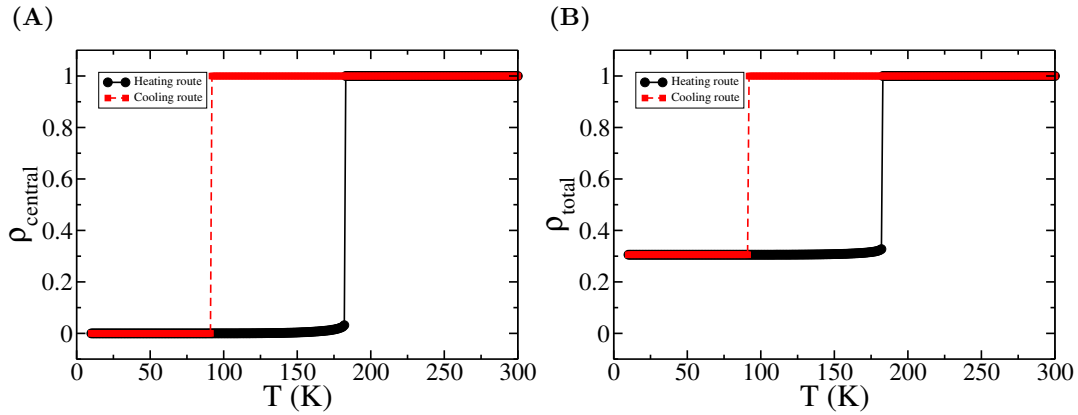


Figure 3: (A) Central ($\rho_{central}$) and (b) Total Fluid Density (ρ_{total}) versus temperature for $L_x = L_y = 7$ nm, $L_z = 13$ nm, $W_c = 3$, and $L = 6.006$ kJ/mol. The black solid curves are the heating routes and the red dashed curve are the cooling routes.

In addition to the phase diagrams discussed above, we analyzed phase diagrams for all simulated parameters. We observed that crystal-fluid transition temperatures in the cooling route (red dashed curves in Figures 2 and 3) are independent of the lattice size, ie, it is a bulk stability limit. Therefore, we define the crystal-fluid transition temperature, T_T , as the transition temperature of the heating route (black solid curves in figures 2 and 3). We emphasize that this definition, although arbitrary, is coherent because we would like to explore the dependence of the variation and not the absolute value of the transition temperature with $L_x = L_y$ e L_z .

The Figure 4 (A) shows the relation between transition temperature and the channel diameter for $W_c = 3$, $L = 6,006$ kJ/mol and $L_z = 13$ nm. We observed that the transition temperature increases with the increase of the channel diameter, until reaches a saturation value for very large sizes. The transition temperature going from 179.5 K, for the smallest channel diameter ($L_x = 5$ nm), to 197.5, for channel diameters greater than 30 nm. These values are always below the bulk water crystal-fluid transition temperature ($T_0 = 273.15$ K). Other values of W_c were analyzed: 1.35, 2.10, 4.05, 5.25, 6.60, 8.10 and 9.75. In all situations the transition temperature T_T behaves similarly to $W_c = 3$: increases with the increase of the channel diameter, until reaches a saturation value, that is below the bulk transition temperature. The T_T will not be equal to T_0 , even for the case where there wall is hydrophobic ($W_c = 0$), since the confinement effect is still great and the latent heat used is still relatively low for this model. Therefore,

it is possible to affirm that the confinement of the water in parallelepiped channels causes a shift in the temperature of transition to temperatures below the bulk temperature transition.

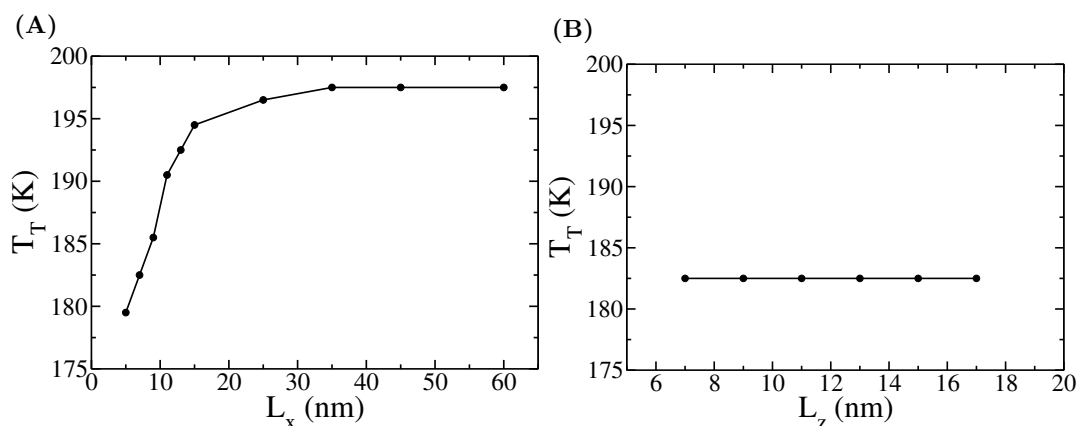


Figure 4: Confined crystal-fluid transition temperature as a function of the channel diameter with $L_z = 13$ nm (A); and crystal-fluid transition temperature as a function of the channel length with $L_x = 7$ nm (B). In both cases, $W_c = 3$ and $L = 6,006$ kJ/mol.

We also found that increasing the channel length, maintaining the channel diameter constant, has no influence on T_T . This result is illustrated in Figure 4(B). The justification for this behavior is that as the length of the channel grows, it approaches the thermodynamic limit. This favors the crystal-fluid transition at T_0 . On the other hand, as the length of the channel increases, increase the interaction with the wall, which favors transitions to temperatures lower than T_0 . These two effects cancel out, and the transition temperature remains constant with increasing channel length. This behavior was observed for all values of W_c , L and L_x analyzed.

The Figure 5 shows the transition temperatures for the three latent heat values studied (6.006, 10 and 20 kJ/mol) with $L_x = 7$ nm and $L_z = 13$ nm. Black solid line is the result for hydrophobic case, and red dashed line is the result for one hydrophilic case ($W_c = 3$). In both cases, the transition temperature increases with the latent heat of fusion. For the hydrophobic case, the transition temperatures range from 212.5 K for $L = 6.006$ kJ/mol to 273.5 K for $L = 10$ kJ/mol, reaching the bulk water transition temperature, $T_0 = 275.15$ K. While for hydrophilic systems the transition temperature does not reach the value of bulk.

4 Conclusions

In this work we studied the dependence of crystal-fluid transition temperature of the water confined with the degree and the nature of confinement. The degree of confinement was varied through changes in channel diameter (L_x) and channel length (L_z). Hydrophobic and hydrophilic walls were simulated.

First we observed that the hydrophobic walls, $W_c = 0$, do not exhibit wetting, ie, do not form a layer of water, in fluid state, in contact with the wall, while in hydrophilic walls, $W_c > 0$ the formation of a fluid

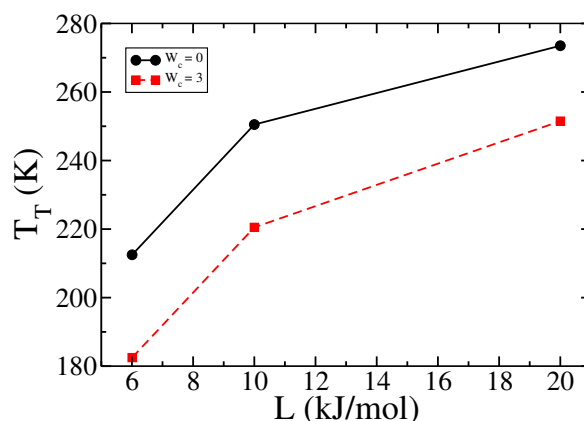


Figure 5: Confined water transition temperature, T_T (K), as a function of latent heat, L (kJ/mol), for (a) $W_c = 0$ and (b) $W_c = 3$ and system size equal to $7 \times 7 \times 13$ nm.

layer at the wall occurs. This result is independent of channel diameter and length.

We also found that for fixed channel length, the transition temperature increases with the channel diameter, until reaches a saturation value. The crystal-fluid temperature transition for confined case were lower than the bulk case in all conditions analyzed. Already for fixed channel diameter, the transition temperature was independent of the channel length.

The study with different values of latent heat showed that transition temperature increases with latent heat. For hydrophobic systems the transition temperatures are larger than transition temperatures for hydrophilic systems. In addition, in the hydrophobic case, the transition temperature approaches to the bulk value for high values of latent heat. While for hydrophilic systems for none of the latent heat values worked, and for none system size, the transition temperature reaches the bulk value.

There is a decrease in the transition temperature with the confinement. The fluid state is more entropic than the crystal state, therefore fluid state exists at higher temperatures. When any form of disorder is introduced into the system, the fluid state is favored. This is the case observed for confined systems. The interaction with the wall causes a disorder in the hydrogen bonds, which leads to the formation of the fluid. This effect is somewhat attenuated for hydrophobic wall, because the wall in this case does not distinguish crystal state of fluid state, adding no disorder to the system. In the case of hydrophilic walls the fluid state is favored. This occurs because hydrophilic walls can make hydrogen bonds with water. To form a hydrogen bond between water-wall, a water-water hydrogen bond is break down. This process favors the fluid state and the system disorder, thereby lowering the crystal-fluid transition temperature.

We used some values of latent heat to try to adjust this parameter appropriately to the model used. Since the water in the lattice is not true water, the latent heat used could not be that of the crystal-fluid transition of the water. Besides the adjustment, the latent heat variation allowed to show that higher latent heat favors transition temperatures closer to the bulk value. This is justified because rising latent heat means that more energy is needed for a transition to occur. In short, this simple model was able to give an overview of the microscopic mechanisms that lead to confined water to form a film on the walls, and to a reduction in the crystal-fluid transition temperature due to confinement.

References

- [1] R. Waler. *Essays of natural experiments*. Johnson Reprint, New York, 1964.
- [2] G. S. Kell. *J. Chem. Eng. Data*, 20:97, 1975.
- [3] C. A. Angell, E. D. Finch, L. A. Woolf, and P. Bach. *J. Chem. Phys.*, 65:3063, 1976.
- [4] R. J. Speedy and C. A. Angell. *J. Chem. Phys.*, 65:851, 1976.
- [5] H. Kanno and C. A. Angell. *J. Chem. Phys.*, 70:4008, 1979.
- [6] C. A. Angell, M. Oguni, and W. J. Sichina. *J. Phys. Chem.*, 86:998, 1982.
- [7] E. Tombari, C. Ferrari, and G. Salvetti. *Chem. Phys. Lett.*, 300:749, 1999.
- [8] F. X. Prielmeier, E. W. Lang, R. J. Speedy, and H.-D. Lüdemann. *Phys. Rev. Lett.*, 59:1128, 1987.
- [9] P. H. Poole, F. Sciortino, U. Essmann, and H. E. Stanley. *Nature (London)*, 360:324, 1992.
- [10] L. Liu, S.-H. Chen, A. Faraone, S.-W. Yen, and C.-Y. Mou. *Phys. Rev. Lett.*, 95:117802, 2005.
- [11] L. Xu, P. Kumar, S. V. Buldyrev, S.-H. Chen, P. Poole, F. Sciortino, and H. E. Stanley. *Proc. Natl. Acad. Sci. USA*, 102:16558, 2005.
- [12] F. A. Santos, J. H. de Queiróz, J. L. Colodette, S. A. Fernandes, V. M. Guimarães, and S. T. Rezende. *Quimica Nova*, 35:1004, 2012.
- [13] Y. P. Zhang and L. R. Lynd. *Biotechnology and bioengineering*, 88:797, 2004.
- [14] Y. Zheng, Z. Pan, R. Zhang, and D. Wang. *Applied Energy*, 86(11):2459, 2009.
- [15] M. Galbe and G. Zacchi. *Pretreatment of Lignocellulosic Materials for Efficient Bioethanol Production*, page 41. 2007.
- [16] F. Marques. *Pesquisa FAPESP*, 163:1620, 2009.
- [17] Y. Sun and J. Cheng. *Bioresource technology*, 83:1, 2002.
- [18] X. Zhao, L. Wang, and D. Liu. *Journal of chemical technology and biotechnology*, 82:1115, 2007.
- [19] M. de Oliveira. *Pesquisa FAPESP*, 200:86, 2012.
- [20] O. V. Petrov and I. Furó. *Prog. Nucl. Magn. Reson. Spectrosc.*, 54:97, 2009.
- [21] C. Driemeier, F. M. Mendes, and M. M. Oliveira. *Cellulose*, 19:1051, 2012.
- [22] G. H Findenegg, S. Jähnert, D. Akcakayiran, and A. Schreiber. *ChemPhysChem*, 9:2651, 2008.

- [23] J. T. Allenhnert, S., F. V. Chavez, G. E. Schaumann, A Schreiber, M SJaonhoff, and G. H. Findenegg. *Physical Chemistry Chemical Physics*, 10:6039, 2008.
- [24] J. Deschamps, F. Audonnet, N. Brodie-Linder, M. Schoeffel, and C. Alba-Simionesco. *Physical Chemistry Chemical Physics*, 12:1440, 2010.
- [25] N. Giovambattista, P. J Rossky, and P. G. Debenedetti. *The Journal of Physical Chemistry B*, 113:13723, 2009.
- [26] E. B Moore, J. T Allen, and V. Molinero. *The Journal of Physical Chemistry C*, 116:7507, 2012.
- [27] N. Giovambattista, P. J Rossky, and P. G. Debenedetti. *Physical review letters*, 102:050603, 2009.
- [28] E. W. Hansen, M. Stöcker, and R. Schmidt. *The Journal of Physical Chemistry*, 100:2195, 1996.
- [29] A. Endo, T. Yamamoto, Y. Inagi, K. Iwakabe, and T. Ohmori. *The Journal of Physical Chemistry C*, 112:9034, 2008.
- [30] D. Kondrashova and R. Valiullin. *The Journal of Physical Chemistry C*, 119:4312, 2015.
- [31] M. J. de Oliveira. *Termodinâmica*. 2005.
- [32] Emily B. Moore, James T. Allen, and Valeria Molinero. *The Journal of Physical Chemistry C*, 116(13):7507–7514, 2012.